Chemical Physics 409 (2012) 49–60

Contents lists available at SciVerse ScienceDirect

Chemical Physics

journal homepage: www.elsevier.com/locate/chemphys

First detection of the silylgermylene (H_3SiGeH) and D4-silylgermylene (D_3SiGeD) molecules in low temperature silane–germane ices

Ada E. Tomosada [a], Seol Kim [a], Yoshihiro Osamura [b], Shu W. Yang [c], Agnes H.H. Chang [c,*], Ralf I. Kaiser [a,*]

[a] Department of Chemistry, University of Hawai'i at Manoa, Honolulu, HI 96822, USA
[b] Kanagawa Institute of Technology, Atsugi 243-0292, Japan
[c] Department of Chemistry, National Dong Hwa University, Shou-Feng, Hualien, Taiwan

ARTICLE INFO

Article history:
Received 21 August 2012
In final form 7 October 2012
Available online 16 October 2012

Keywords:
Ionizing radiation of energetic electrons
Kinetic studies
Online and *in situ* infrared spectroscopy
Silylgermylene (H_3SiGeH) detection

ABSTRACT

The thermodynamically most stable $GeSiH_4$ isomer – silylgermylene ($H_3SiGeH(X^1A')$) – and its perdeuterated counterpart were detected for the first time via infrared spectroscopy in low temperature silane (SiH_4) – germane (GeH_4) and D4-silane – D4-germane ices upon irradiation with energetic electrons through the ν_5 and ν_3 fundamentals at 860 cm^{-1} and at 1309 cm^{-1}, respectively. Our kinetic studies suggest that silylgermylene is formed via decomposition of chemically activated silylgermane (H_3SiGeH_3) precursors.

1. Introduction

Recent years have shown an increasing innovation in silicon–germanium related devices such as semiconductors [1], silicon–germanium nanowires [2,3], modulation doped field effect transistors (MODFET) [4,5], resonant tunneling diodes (RTD), infrared detectors [6,7], and light emitting diodes [8]. Silicon–germanium semiconductors play a crucial role in the development of hetero-junction bipolar transistors (HBT) with HBTs contributing to vital progress in the wireless communication market [9,10]. HBTs are also highly resistant to a wide range of temperatures from 93 to 393 K and ionizing radiation from the Solar Wind and the Galactic Cosmic Radiation (GCR); these properties make HBTs important building blocks in space electronics design, since they require little radiation shielding [11]. In 1988, the very first functional HBT was reported employing molecular beam epitaxial (MBE) to grow silicon–germanium thin films onto the silicon substrate [12]. Since then, various techniques have been developed such as chemical vapor deposition (CVD) at low temperature for the growth of the SiGe epitaxial layer [13]. As of today, CVD technology presents the preferred technique for the production of silicon–germanium HBTs with the production processes still being refined. Here, germanium- and silicon-bearing species such as SiH_x and GeH_x ($x = 1–3$) and silicon–germanium clusters of various degree of hydrogenation, i.e., $GeSiH_x$ ($x = 0–6$), have been suggested to represent major growth species to produce germanium–silicon films. To further optimize the production processes, a firm identification of the growth-limiting reactions for the production of germanium–silicon films is required. This necessitates a rigorous knowledge of the time-dependent concentration profiles of silicon–germanium-bearing species in chemical vapor deposition processes as derived spectroscopically. However, the spectroscopy of $GeSiH_x$ is largely undetermined.

What is currently known on properties of $GeSiH_x$ ($x = 0–6$) species? The majority of the computational and experimental studies focused on silylgermane (H_3SiGeH_3). This molecule was first identified by Spanier and Mac-Diarmid using electric discharge of silane–germane gas mixtures [14]. Since then, a directed synthesis of silylgermane has been reported [15]. Further experimental studies were conducted on the vibrational spectra and its deuterated counterparts both in the solid state and in the gas phase by Lannon et al. [16] and in the liquid state by Mohan et al. [17,18]. Bond lengths and bond angles in silylgermane were characterized by Oberhammer et al. [19]. Further, Gaspar et al. [20] investigated the reactions of germanium atoms recoiling from the $^{76}Ge(n, 2n)^{75}Ge$ nuclear transformation in the gas phase. The authors proposed that silylgermane is formed through insertion reaction of a $^{75}GeH_2$ transient species via Eq. (1). Also, Saalfeld et al. determined the enthalpy of formation of silylgermane to be 31 kJ mol^{-1} [21]. *Ab initio* calculations of the vibrational frequencies were conducted as well [22,23]. Besides the silylgermane molecule, only limited studies were conducted on the $GeSiH_x$ ($x = 1–5$) species. *Ab initio* calculations were carried out to characterize structural isomers of $SiGeH_4$. Grev et al. suggested silylgermylene,

* Corresponding authors. Tel.: +1 808 956 5731; fax: +1 808 956 5908.
E-mail addresses: hhchang@mail.ndhu.edu.tw (A.H.H. Chang), ralfk@hawaii.edu (R.I. Kaiser).

0301-0104/$ - see front matter © 2012 Elsevier B.V. All rights reserved.
http://dx.doi.org/10.1016/j.chemphys.2012.10.002

$H_3SiGeH(X^1A')$, to be the lowest lying isomer, 26 kJ below the trans-bent doubly bonded germasilene, $H_2SiGeH_2(X^1A')$ structure and 31 kJ lower than planar germasilene $H_2SiGeH_2(X^1A_1)$ [24]. They also predicted the dissociation bond energy of the silicon–germanium single bond of silylgermane to be 93 kJ mol^{-1} higher than the silicon–germanium double bond of silylgermylene due to the divalent state stabilization energy (DSSE).

$$^{75}GeH_2 + SiH_4 \rightarrow H_3{}^{75}GeSiH_3 \quad (1)$$

However, despite their potential role as key-growth species in germanium–silicon CVD processes, until now, no hydrogen deficient, neutral $GeSiH_x$ (x = 1–5) species has been identified experimentally in the gas or condensed phase. This is in strong contrast to the dinuclear Si_2H_x and Ge_2H_x molecules, whose vibrational spectra have been characterized for disilyl (Si_2H_5), silylsilylene (H_3SiSiH), disilene (H_2SiSiH_2), and disilenyl (H_2SiSiH) [25,26], as well as digermyl (Ge_2H_5), digermene (Ge_2H_4), and digermenyl (Ge_2H_3) [27,28]. In this paper, we present the very first experimental evidence in combination with theoretical studies of the radiation-induced formation of silylgermane (H_3SiGeH_3) and of the hitherto elusive silylgermylene (H_3SiGeH) molecule along with their deuterated counterparts in electron-irradiated low temperature silane–germane matrices.

2. Experimental

Experiments were conducted in an ultrahigh vacuum (UHV) stainless steel chamber described in detail in Ref. [25]. The chamber can be pumped down to the medium 10^{-11} Torr range by a magnetically suspended turbo molecular pump backed by an oil-free scroll pump. Interfaced to the chamber is a two-staged closed cycle helium refrigerator holding a polished silver crystal. The crystal is cooled to 12.0 ± 0.2 K and acts as a substrate for the solid ices. A silane (SiH_4; 99.99%, Aldrich) – germane (GeH_4; 99.99%, Aldrich) gas mixture was prepared as a 1:1 mixture as was the D4-silane (99.99%, Aldrich) – D4-germane (99.99%, Voltaix) mixture. The gas mixture is introduced via a Balzers UDV 235 thermovalve into the main chamber by passing through a linear transfer mechanism and a gas capillary array (GCA), before condensing onto the crystal held at 12 K. The depositions were carried out at pressure of 10^{-7} Torr for 10 min. The absorptions of the silane–germane frost are complied in Table 1. The infrared absorption features of 2189 cm^{-1} for silane and 2090 cm^{-1} for germane were integrated and the ice thickness calculated. Using a modified Lambert–Beer relationship [29], densities of the individual solids of 0.77 g cm^{-3} and 1.75 g cm^{-3}, for silane and germane, respectively, absorption coefficients of 4.7×10^{-17} and 5.5×10^{-17} cm molecules^{-1} [30], the calculated optical thickness of the layers were 24 ± 15 and 29 ± 2 nm for silane and germane, respectively. The ices were irradiated at 12 K with 5 keV electrons generated in an electron source at beam currents of 1000 nA and 100 nA for 60 min by scanning the electron beam over the target area of 3.0 ± 0.2 cm^2. The Nicolet 6700 Fourier transform infrared spectrometer (6000–400 cm^{-1}) was used for on-line and *in situ* monitoring of the chemical modifications of the solid samples; the spectrometer operates in an absorption–refection–absorption mode with reflection angle α = 75° and resolution 4 cm^{-1}.

3. Theoretical methods

The energetics of isomers of $GeSiH_x$ (x = 1–6) were characterized by *ab initio* electronic structure calculations. The optimized geometries and harmonic frequencies were computed at the level of the hybrid density functional theory, B3LYP/6-311G(d,p) [31–34]; their energies were refined further at the CCSD(T)/6-311G(d,p) level of theory with B3LYP/cc-pVTZ zero-point energy corrections [35–38]. While it is found to be a transition state on the surface of B3LYP/6-311G(d,p), with MP2/6-311G(d,p) the geometry and frequencies of the isomer $H_3SiGeH(X^1A')$ were obtained. The GAUSSIAN03 program [39] was employed in the calculations.

Table 1
Infrared absorptions of the silane, D4-silane, germane and D4-germane frost. (sh: shoulder) α, β,γ denote lattice modes of the samples.

Frequency (cm^{-1})	Frequency (cm^{-1})	Assignment	Ref.
Silane	D4-silane		
4351		$2\nu_3$	[25,26]
4284	3118	$\nu_1 + \nu_3$	[25,26]
3128	2246	$\nu_2 + \nu_3$	[25,26]
3065	2173	$\nu_3 + \nu_4$	[25,26]
2189	1596	$\nu_3 + \alpha$	[25,26]
2167	1583	ν_3	[25,26]
1870	1354	$\nu_2 + \nu_4 + \alpha$	[25,26]
1848	1340	$\nu_2 + \nu_4$	[25,26]
960	683	ν_2	[25,26]
913	674	$\nu_4 + \alpha$	[25,26]
881	652	ν_4	[25,26]
Germane	D4-germane		
4193		$2\nu_3$	[27,28]
4123	2981	$\nu_1 + \nu_3$	[27,28]
3003	2158 (sh)	$\nu_2 + \nu_3\nu_3 + \alpha$	[27,28]
2109	1520	$\nu_3 + \beta$	[27,28]
2090	1507	$\nu_3 + \alpha$	[27,28]
1722	1233	$\nu_2 + \nu_4$	[27,28]
960	683	$\nu_4 + \gamma$	[27,28]
915	660	ν_2	[27,28]
823	616	$\nu_4 + \beta$	[27,28]
803	596	$\nu_4 + \alpha$	[27,28]
795	575	ν_4	[27,28]

4. Theoretical results

The relative energies for the optimized geometric structures for $SiGeH_x$ (x = 1–6) species are compiled in Table 2. In order to identify the silicon–germanium bearing compounds and their deuterated counterparts formed in the silane–germane ices upon electron irradiation, the vibrational fundamentals of the $SiGeH_x$ (x = 1–6) as well as their integrated absorption coefficients were computed as provided in Table 3. The geometries of the $SiGeH_x$ (x = 1–6) species are depicted in Fig. 1.

In preceding studies done by Sillars et al. [25] and Carrier et al. [28] the optimized geometries of the lowest energy structures were the staggered conformation for the Si_2H_6 and Ge_2H_6 of the x = 6 species, as was found for the $SiGeH_6$ in the present study (Fig. 1(a)). However, in the previous studies, a higher energy Si_2H_6 isomer ($H_3SiHSiH_2$) was found; this structure formally presents a complex between the silane (SiH_4) and the SiH_2 radical unit. The corresponding isomer for the Ge_2H_6 species, $H_3GeHGeH_2$ was also reported. In this investigation, employing the B3LYP/6-311G(d,p), a second $SiGeH_6$ isomer was also found; but unlike the $H_3GeHGeH_2(X^1A)$ structure, which indicates that a vacant p-orbital of the GeH_2 unit is acting as an electron acceptor of the electrons of the Ge–H bond in GeH_4, the $H_3SiHGeH_2(X^1A)$ presents a monobridged structure.

Considering x = 5 species, the lowest energy isomer for $SiGeH_5$ species presents the $H_3SiGeH_2(X^2A')$ molecule, which lies 17.1 kJ mol^{-1} below the $H_2SiGeH_3(X^2A')$ (Fig. 1(b)). This energy difference can be explained by the larger silicon–hydrogen bond energy, typically 378 kJ mol^{-1} [40], compared to the germane–hydrogen bond energy of around 343 kJ mol^{-1} [41]. In previous studies by Sillars et al. [25] and Carrier et al. [28] the optimized geometries of the lowest energy isomers for the Si_2H_5 and Ge_2H_5

Table 2
The computed relative energies of $SiGeH_x$ isomers (x = 1–6).

Species	B3LYP method [(a)] (kJ mol^{-1})	CCSD(T) method [(b)] (kJ mol^{-1})
$SiGeH_6$		
H_3SiGeH_3 ($^1A_1$) [1]	0.0	0.0
$H_3SiHGeH_2$ (^1A) [2]	127.5	133.8
$SiGeH_5$		
H_3SiGeH_2 ($^2A'$) [1]	0.0	0.0
H_2SiGeH_3 ($^2A'$) [2]	16.3	17.1
$SiGeH_4$		
H_3SiGeH ($^1A'$) [1]	0.0	0.0
H_2SiGeH_2 ($^1A'$) [2]	23.7	15.0
$HSiGeH_3$ ($^1A'$) [3]	68.9	64.3
trans-HSiHHGeH ($^1A'$) [4]	77.2	76.8
cis-HSiHHGeH ($^1A'$) [5]	85.9	86.2
$SiGeH_3$		
H_3SiGe ($^2A''$) [1]	0.0	0.0
H_2SiGeH ($^2A''$)[2]	17.5	31.3
trans-HSiHGeH (^2A) [3]	51.6	62.8
$HSiGeH_2$ (^2A) [4]	56.9	65.6
HSiHHGe ($^2A'$) [5]	76.6	78.8
cis-HSiHGeH (^2A) [6]	75.8	87.9
SiGe H_3 ($^2A''$) [7]	88.4	87.9
SiHHGeH ($^1A'$) [8]	98.5	104.5
$SiGeH_2$		
SiH_2Ge ($^1A'$) [1]	0.0	0.0
H_2SiGe ($^1A_1$) [2]	16.3	17.1
HSiHGe ($^1A'$) [3]	23.5	23.4
SiHGeH ($^1A'$) [4]	55.5	51.5
HSiGeH ($^1A'$) [5]	77.8	64.7
$SiGeH_2$ ($^1A_1$) [6]	74.2	72.5
SiGeH		
SiHGe ($^2A'$) [1]	0.0	0.0

Notes: optimized structures of $SiGeH_x$ isomers are shown in Fig. 1.
[(a)] Zero-point energies corrected at the same B3LYP/6-311G(d,p) level.
[(b)] CCSD(T)/6-311G(d,p) energies based on the B3LYP/6-311G(d,p) optimized structures.

species were H_3SiSiH_2 and H_3GeGeH_2, respectively. It is interesting to note that although the $HSiHSiH_3$ and $HGeHGeH_3$ hydrogen-bridged isomers were found to be higher energy isomers, the corresponding $H_3SiHGeH$ or $H_3GeHSiH$ geometries could not be identified in the present investigation.

We now compare the optimized geometries of the lowest energy isomers of Si_2H_x, Ge_2H_x, and $SiGeH_x$ (x = 4,3). In previous works by Sillars et al. [26] and Carrier et al. [27] the trans-bent $H_2SiSiH_2(X^1A_g)$ as well as the trans-bent $H_2GeGeH_2(X^1A_g)$ were found to be the lowest energy isomers for x = 4. In the present work, the silylgermylene $H_3SiGeH(X^1A')$ shown in Fig 2(c) ranges 15.0 kJ mol^{-1} below the trans-bent $H_2SiGeH_2(X^1A')$ utilizing the CCSD(T)/6-311G(d,p) level of theory (Table 2). This can be rationalized by Grev et al. [24] Using their calculated bond energies, the isomerization of the germasilene (H_2GeSiH_2) to silylgermylene (H_3SiGeH) is exoergic by 34 kJ mol^{-1}. The isomerization energy of H_2SiSiH_2 to H_3SiSiH is however endoergic by 12 kJ mol^{-1}. For x = 3, a similar pattern emerges. The H_2SiSiH [26] and H_2GeGeH [27] isomers represent the lowest energy structures, whereas in the present study, the H_3SiGe has the lowest energy due to the stronger silicon–hydrogen bond as compared to the germanium–hydrogen bond, lying 31.3 kJ mol^{-1} below the H_2SiGeH isomer. The di-bridged SiH_2Ge structure has a similar geometry as the lowest energy Ge_2H_2 and Si_2H_2 isomers [42,43]. The mono-bridged SiHGe is the only optimized geometry for the x = 1. The bridged Ge_2H was studied by Gopakumar et al. [44].

5. Experimental results

The infrared spectra of the silane–germane frosts before the irradiation are shown in Fig 2(a). After one hour of irradiation new absorption features appeared. These were first assigned to the known Si_2H_x and Ge_2H_x (x = 1–6) species along with their deuterated counterparts according to the experimental literature values [25–28]. The infrared spectroscopic studies confirmed previous works done on the pure silane [25,26] and germane [27,28] matrices. The Si_2H_6 ν_6 at 820 cm^{-1}, H_3SiSiH_2 ν_6 at 844 cm^{-1} [25], H_3SiSiH ν_5 869 cm^{-1}, H_2SiSiH ν_5 636 cm^{-1} [26] as well as their deuterated counterparts Si_2D_6 ν_5 at 1531 cm^{-1}, D_3SiSiD_2 ν_6 at 621 cm^{-1} [25], D_3SiSiD ν_5 at 635 cm^{-1}, D_2SiSiD ν_4 at 683 cm^{-1} [26], as compiled in Table 4, were identified in the silane–germane ices. Also, the Ge_2H_6 ν_6 at 752 cm^{-1} and ν_{11} at 869 cm^{-1}, H_2GeGeH_3 ν_6 at 766 cm^{-1} [28], H_3GeGeH ν_5 at 780 cm^{-1}, H_2GeGeH ν_3 at 1819 cm^{-1} [27], as well as their deuterated counterparts Ge_2D_6 ν_6 at 530 cm^{-1} and ν_{11} at 626 cm^{-1}, D_2GeGeD_3 ν_4/ν_{12} at 609 cm^{-1} [28], D_2GeGeD_2 ν_5 at 1481 cm^{-1}, D_3GeGeD ν_5 at 557 cm^{-1}, D_2GeGeD ν_3 at 1319 cm^{-1} [27] were monitored as shown in Table 4.

Besides the Ge_2H_x and Si_2H_x species as outlined above, additional absorption features were present in the irradiated samples (Fig. 2), which could not be attributed to any of the Ge_2H_x and Si_2H_x (x = 1–6) molecules. Therefore, we compared scaled, calculated absorption features of various $SiGeH_x$ (x = 1–6) (Table 3; Fig. 1) molecules with the experimental observations (Fig. 2). These absorption peaks of the newly observed molecules are compiled in Table 5. The infrared spectroscopic studies suggest the formation of the silylgermane ($H_3SiGeH_3(X^1A_1)$) (Fig. 1(a)) during the one hour irradiation of the silane (SiH_4) – germane (GeH_4) frost at 12 K. The absorption features at 2062 cm^{-1}, as shown in Fig 2(b), was assigned to the ν_2 mode as predicted via B3LYP/6-311G(d,p) theoretical calculations (Table 3) utilizing a recommended scaling factor of 0.97. Note that the harmonic approximation employed for

Table 3
Unscaled vibrational frequencies (cm^{-1}) and infrared intensities ($km\ mol^{-1}$) for $SiGeH_x$ and $SiGeD_x$ ($x = 1–6$) species obtained with B3LYP/6-311G(d,p). Note: [1] H_3SiGeH and D_3SiGeD are evaluated with MP2/6-311G(d,p).

Mode		Frequency	Intensity	Frequency	Intensity	Characterization
[1]		H3SiGeH3 (^{1}A1)		D_3SiGeD_3 ($^1A_1$)		
ν_1	a_1	2217	62.26	1577	36.60	SiH_3 sym. str.
ν_2	a_1	2126	79.36	1507	42.05	GeH_3 sym. str.
ν_3	a_1	903	118.11	667	84.99	SiH_3 umbrella
ν_4	a_1	797	412.64	575	195.95	GeH_3 umbrella
ν_5	a_1	344	0.32	330	1.19	GeSi str.
ν_6	a_2	126	0.00	89	0.00	Torsion
ν_7	e	2229	113.39	1611	63.37	SiH_3 asym. str.
ν_8	e	2134	110.47	1522	57.99	GeH_3 asym. str.
ν_9	e	954,954	53.68,53.68	684,684	28.83,28.83	SiH_3 deformation
ν_{10}	e	894,894	27.61,27.61	635,635	12.88,12.88	GeH_3 deformation
ν_{11}	e	602,602	0.00,0.00	451,450	0.01,0.01	GeH_3, SiH_3 rock
ν_{12}	e	374,374	22.12,22.12	267,267	11.04,11.04	GeH_3, SiH_3 rock
ν_{13}	e	2229	113.40	1611	63.38	SiH_2 asym. str.
ν_{14}	e	2134	110.47	1522	57.99	GeH_2 asym. str.
[2]		$H_3SiHGeH_2$ (^{1}A)		$D_3SiDGeD_2$ (^{1}A)		
ν_1	a	111	0.89	90	0.17	GeSi str.
ν_2	a	128	0.21	104	0.79	Torsion
ν_3	a	188	0.50	135	0.22	Torsion
ν_4	a	382	32.29	285	16.71	GeH_2, SiH_4 rock
ν_5	a	554	12.07	400	4.57	GeH_2, SiH_4 rock
ν_6	a	577	41.57	420	24.69	GeH_2, SiH_4 rock
ν_7	a	873	134.23	628	37.51	SiH_3 umbrella
ν_8	a	886	276.37	650	165.00	SiH_3 umbrella
ν_9	a	922	45.49	658	26.11	GeH_2 scissor
ν_{10}	a	945	63.89	679	27.76	SiH_4 deformation
ν_{11}	a	958	42.40	687	35.00	SiH_4 deformation
ν_{12}	a	1120	47.43	801	26.49	SiH_2 scissor
ν_{13}	a	1867	378.08	1331	169.72	GeH str.
ν_{14}	a	1880	255.34	1346	160.03	Bridge HSi str.
ν_{15}	a	1902	309.60	1355	164.34	GeH_2 asym. str.
ν_{16}	a	2247	68.94	1602	39.72	SiH_3 sym. str.
ν_{17}	a	2275	57.10	1641	41.83	SiH_3 asym. str.
ν_{18}	a	2298	53.03	1661	36.99	SiH_2 asym. str.
[1]		H_3SiGeH_2 (^{2}A′)		D_3SiGeD_2 (^{2}A′)		
ν_1	a′	2227	83.34	1604	54.32	SiH_3 asym. str.
ν_2	a′	2200	84.57	1570	42.59	SiH_3 sym. str.
ν_3	a′	2079	106.49	1477	54.97	GeH_2 sym. str.
ν_4	a′	948	56.27	680	23.05	SiH_3 deformation
ν_5	a′	900	118.58	661	100.93	SiH_3 umbrella
ν_6	a′	837	340.77	601	142.34	GeH_2 scissor
ν_7	a′	569	14.07	424	6.59	GeH_2 umbrella, SiH_3 rock
ν_8	a′	393	15.55	273	8.44	GeH_2 umbrella, SiH_3 rock
ν_9	a′	328	1.65	325	0.62	GeSi str.
ν_{10}	a″	2236	105.13	1616	58.94	SiH_3 asym. str.
ν_{11}	a″	2108	133.16	1504	68.17	GeH_2 asym. str.
ν_{12}	a″	950	44.17	681	32.55	SiH_3 deformation
ν_{13}	a″	604	0.93	450	0.36	GeH_2 rock, SiH_3 rock
ν_{14}	a″	373	83.34	265	8.74	GeH_2 rock, SiH_3 rock
ν_{15}	a″	112	0.12	79	0.06	Torsion
[2]		H_2SiGeH_3 (^{2}A′)		D_2SiGeD_3 (^{2}A′)		
ν_1	a′	2184	82.86	1562	46.14	SiH_2 sym. str.
ν_2	a′	2132	97.50	1517	54.39	GeH_3 asym. str.
ν_3	a′	2104	106.94	1496	52.39	GeH str.
ν_4	a′	927	76.96	672	41.49	SiH_2 scissor
ν_5	a′	888	39.32	632	20.27	GeH_3 deformation
ν_6	a′	803	299.68	577	151.39	GeH_3 umbrella
ν_7	a′	583	30.87	440	17.22	GeH_3 rock, SiH_2 umbrella
ν_8	a′	400	18.78	285	9.24	GeH_3 rock, SiH_2 umbrella
ν_9	a′	342	0.75	334	1.69	GeSi str.
ν_{10}	a″	2212	125.89	1600	64.87	SiH_2 asym. str.
ν_{11}	a″	2138	97.84	1525	52.72	GeH_2 asym. str.
ν_{12}	a″	891	32.2	633	16.39	GeH_3 deformation
ν_{13}	a″	600	0.71	446	0.39	GeH_3, SiH_2 rock
ν_{14}	a″	382	16.93	271	8.47	GeH_3, SiH_2 rock
ν_{15}	a″	123	0.40	87	0.20	Torsion
[1]		H_3SiGeH (^{1}A′)		D_3SiGeD (^{1}A′)		
ν_1	a′	2302	133.49	1661	75.76	SiH_3 asym. str.
ν_2	a′	2276	94.78	1621	52.76	SiH_3 sym. str.

Table 3 (*continued*)

Mode		Frequency	Intensity	Frequency	Intensity	Characterization
ν_3	a′	1987	270.90	1415	136.99	GeH str.
ν_4	a′	976	73.02	701	58.54	SiH_3 deformation
ν_5	a′	912	345.99	675	150.81	SiH_3 umbrella
ν_6	a′	697	44.34	511	23.38	GeH bend, SiH_3 deformation
ν_7	a′	412	23.35	317	16.51	GeH bend, SiH_3 deformation
ν_8	a′	318	8.06	286	7.51	GeSi str.
ν_9	a″	2285	122.81	1651	71.63	SiH_3 asym. str.
ν_{10}	a″	999	53.87	716	29.30	SiH_3 deformation
ν_{11}	a″	391	34.58	285	18.18	SiH_3 deformation
ν_{12}	a″	92	5.86	66	2.92	Torsion
[2]		H_2SiGeH_2 ($^1A'$)		D_2SiGeD_2 ($^1A'$)		
ν_1	a′	2209	75.39	1581	41.20	SiH_2 sym. str.
ν_2	a′	2119	84.07	1506	44.50	GeH_2 sym. str.
ν_3	a′	948	92.52	692	44.53	SiH_2 scissor
ν_4	a′	876	109.09	626	57.86	GeH_2 scissor
ν_5	a′	502	1.44	428	1.94	GeSi str.
ν_6	a′	404	37.07	310	4.97	SiH_2 out of plane
ν_7	a′	353	2.78	281	15.47	GeH_2 out of plane
ν_8	a″	2236	97.30	1617	50.69	SiH_2 asym. str.
ν_9	a″	2140	94.06	1527	49.16	GeH_2 asym. str.
ν_{10}	a″	587	0.05	438	0.03	SiH_2, GeH_2 rock
ν_{11}	a″	506	0.06	358	0.03	Torsion
ν_{12}	a″	331	17.02	235	8.59	SiH_2, GeH_2 rock
[3]		$HSiGeH_3$ ($^1A'$)		$DGeCD_3$ ($^1A'$)		
ν_1	a′	2119	162.34	1510	94.28	GeH_3 asym. str.
ν_2	a′	2086	111.7	1481	61.03	GeH_3 sym. str.
ν_3	a′	2038	176.7	1466	78.10	SiH str.
ν_4	a′	879	39.38	624	21.36	GeH_3 deformation
ν_5	a′	793	221.28	570	105.88	GeH_3 umbrella
ν_6	a′	699	59.51	514	38.26	SiH bend
ν_7	a′	397	17.61	273	6.11	GeH_3 deformation
ν_8	a′	311	4.53	320	7.46	GeSi str.
ν_9	a″	2095	122.5	1494	64.56	GeH_3 asym. str.
ν_{10}	a″	895	27.57	637	14.34	GeH_3 deformation
ν_{11}	a″	357	23.19	256	12.00	GeH_3 deformation
ν_{12}	a″	77	6.55	55	3.32	Torsion
[4]		*trans*-HSiHHGeH ($^1A'$)		*trans*-DSiDDGeD ($^1A'$)		
ν_1	a′	2055	232.48	1478	120.35	SiH str.
ν_2	a′	1894	261.71	1349	135.35	GeH str.
ν_3	a′	1625	185.23	1155	104.03	SiHH sym. str.
ν_4	a′	1287	673.23	917	340.54	GeHH sym. str.
ν_5	a′	843	97.66	612	40.62	SiH bend
ν_6	a′	757	48.00	544	30.27	GeH bend
ν_7	a′	345	0.10	312	1.47	SiGe str.
ν_8	a′	264	4.64	205	2.38	SiHHGe out of plane
ν_9	a″	1451	29.88	1039	16.28	SiHH asym. str.
ν_{10}	a″	1091	19.97	776	10.32	GeHH asym. str.
ν_{11}	a″	850	7.93	608	3.77	Torsion
ν_{12}	a″	628	10.65	448	5.17	Torsion
[5]		*cis*-HSiHHGeH ($^1A'$)		*cis*-DSiDDGeD ($^1A'$)		
ν_1	a′	2073	237.17	1491	120.49	SiH str.
ν_2	a′	1927	219.99	1373	114.75	GeH str.
ν_3	a′	1590	127.08	1129	75.32	SiHH sym. str.
ν_4	a′	1261	1065.35	902	543.04	GeHH sym. str.
ν_5	a′	868	41.85	623	21.01	SiH, GeH bend
ν_6	a′	681	50.71	492	22.38	SiH, GeH bend
ν_7	a′	370	0.10	262	0.09	SiHHGe out of plane
ν_8	a′	305	3.18	304	4.15	SiGe str.
ν_9	a″	1363	26.63	977	14.35	SiHH asym. str.
ν_{10}	a″	1101	25.33	783	12.84	GeHH asym. str.
ν_{11}	a″	837	13.14	596	6.06	Torsion
ν_{12}	a″	581	0.95	415	0.59	Torsion
[1]		H_3SiGe ($^2A''$)		D_3SiGe ($^2A''$)		
ν_1	a′	2186	123.80	1572	70.83	SiH_3 asym. str.
ν_2	a′	2157	83.10	1541	45.16	SiH_3 sym. str.
ν_3	a′	954	65.70	685	40.66	SiH_3 deformation
ν_4	a′	863	297.12	638	138.86	SiH_3 umbrella
ν_5	a′	348	20.20	305	13.78	SiH_3 rock
ν_6	a′	267	14.20	217	11.69	SiGe str.
ν_7	a″	2190	117.16	1582	65.45	SiH_3 asym. str.

(*continued on next page*)

Table 3 (*continued*)

Mode		Frequency	Intensity	Frequency	Intensity	Characterization
ν_8	a″	916	45.00	657	23.27	SiH_3 deformation
ν_9	a″	367	6.54	270	3.14	SiH_3 rock
[2]		H_2SiGeH ($^2A''$)		D_2SiGeD ($^2A''$)		
ν_1	a′	2204	123.72	1593	66.84	SiH_2 asym. str.
ν_2	a′	2179	123.16	1560	63.40	SiH_2 sym. str.
ν_3	a′	1885	254.45	1342	128.19	GeH str.
ν_4	a′	966	110.82	701	48.84	SiH_2 scissor
ν_5	a′	662	29.93	487	18.02	GeH bend, SiH_2 rock
ν_6	a′	343	11.30	336	10.77	SiGe str.
ν_7	a′	374	7.26	269	4.75	SiH_2 rock
ν_8	a″	360	5.95	264	3.48	Out of plane
ν_9	a″	160	0.25	116	0.15	Torsion
[3]		$HSiGeH_2$ (^2A)		$DSiGeD_2$ (^2A)		
ν_1	a	2087	191.24	1489	118.33	GeH asym. str.
ν_2	a	2056	135.31	1460	72.83	GeH sym. str.
ν_3	a	2037	150.18	1466	52.42	SiH str.
ν_4	a	882	83.09	631	39.18	GeH_2 scissor
ν_5	a	674	29.13	494	18.97	SiH bend
ν_6	a	394	2.76	266	2.75	Out of plane
ν_7	a	346	10.25	249	5.47	GeH_2 rock
ν_8	a	340	7.08	351	3.45	SiGe str.
ν_9	a	159	7.00	118	4.08	Torsion
[4]		*trans*-HSiHGeH (^2A)		*trans*-DSiDGeD (^2A)		
ν_1	a	2089	195.47	1503	102.12	SiH str.
ν_2	a	1939	221.80	1381	113.27	GeH str.
ν_3	a	1506	118.17	1080	59.57	Bridge H str.
ν_4	a	954	101.42	679	50.02	Bridge H shift
ν_5	a	700	8.18	507	3.14	HSiGeH bend
ν_6	a	636	52.80	459	28.31	Bridge H shift
ν_7	a	597	10.51	430	6.06	HSiGeH torsion
ν_8	a	351	5.20	337	2.25	SiGe str.
ν_9	a	324	0.57	238	1.53	HSiGeH bend
[5]		*cis*-HSiHGeH (^2A)		*cis*-DSiDGeD (^2A)		
ν_1	a	2087	185.00	1503	93.92	SiH str.
ν_2	a	1841	206.25	1311	104.90	GeH str.
ν_3	a	1548	129.23	1110	64.06	Bridge H str.
ν_4	a	887	140.14	632	68.19	Bridge H shift
ν_5	a	755	27.10	536	14.59	Bridge H shift
ν_6	a	585	48.86	431	31.19	HSiGeH bend
ν_7	a	506	19.51	377	10.55	HSiGeH torsion
ν_8	a	373	3.94	264	2.43	HSiGeH bend
ν_9	a	311	6.94	299	4.32	SiGe str.
[6]		HSiHHGe ($^2A'$)		DSiDDGe($^2A'$)		
ν_1	a′	2044	183.03	1471	96.48	SiH str.
ν_2	a′	1641	173.49	1167	95.36	Bridge HH sym. str.
ν_3	a′	1197	641.1	855	322.39	HGeH sym. str.
ν_4	a′	815	88.24	589	40.65	HSi bend
ν_5	a′	346	1.90	316	5.51	HSiHH deformation
ν_6	a′	249	4.15	192	1.56	HSiHH deformation
ν_7	a″	1467	26.62	1051	14.20	Bridge HH asym. str.
ν_8	a″	1034	17.00	735	8.74	HGeH asym. str.
ν_9	a″	811	12.34	580	5.82	HSiHH deformation
[7]		SiHHGeH ($^2A'$)		SiDDGeD ($^2A'$)		
ν_1	a′	1853	298.8	1320	153.24	GeH str.
ν_2	a′	1598	131.61	1139	74.33	Bridge HH sym. str.
ν_3	a′	1181	419.46	845	209.32	HGeH sym. str.
ν_4	a′	697	91.04	506	48.93	HGe bend
ν_5	a′	499	1.59	397	0.35	HGeHH deformation
ν_6	a′	109	0.03	97	0.02	HGeHH deformation
ν_7	a″	1472	74.39	1054	37.9	Bridge HH asym. str.
ν_8	a″	1015	3.04	720	1.50	HGeH asym. str.
ν_9	a″	358	0.51	255	0.22	HSiHH deformation
[8]		$SiGeH_3$ ($^2A''$)		$SiGeD_3$($^2A''$)		
ν_1	a′	2089	139.92	1486	73.66	GeH_3 asym. str.
ν_2	a′	2054	95.74	1460	49.00	GeH_3 sym. str.
ν_3	a′	887	46.2	631	24.35	GeH_3 deformation
ν_4	a′	785	235.17	564	116.32	GeH_3 umbrella
ν_5	a′	335	13.15	320	8.43	GeSi str.
ν_6	a′	267	19.32	203	12.81	GeH_3 rock

Table 3 (*continued*)

Mode		Frequency	Intensity	Frequency	Intensity	Characterization
ν_7	a″	2089	142.37	1490	74.19	GeH_3 asym. str.
ν_8	a″	860	31.00	612	15.79	GeH_3 deformation
ν_9	a″	341	8.22	248	4.12	GeH_3 rock
[1]		SiH_2Ge ($^1A'$)		SiD_2Ge ($^1A'$)		
ν_1	a′	1554	40.12	1107	23.36	H-H str.
ν_2	a′	1054	304.79	762	148.16	SiH_2 str.
ν_3	a′	870	75.53	628	43.65	GeH_2 str.
ν_4	a′	406	1.40	398	2.08	Ge-Si str.
ν_5	a″	1481	35.82	1058	18.22	HGeH rock
ν_6	a″	928	0.01	661	0.00	HSi, HGe str.
[2]		H_2SiGe ($^1A_1$)		D_2SiGe ($^1A_1$)		
ν_1	a_1	2187	61.56	1565	31.10	SiH_2 sym. str.
ν_2	a_1	895	65.75	659	25.56	SiH_2 scissor
ν_3	a_1	410	11.36	394	14.13	SiGe str.
ν_4	b_1	331	2.46	248	1.46	Out of plane
ν_5	b_2	2217	79.92	1604	44.31	SiH_2 asym. str.
ν_6	b_2	254	22.14	188	11.88	SiH_2 rock
[3]		HSiHGe ($^1A'$)		DSiDGe ($^1A'$)		
ν_1	a′	2178	85.60	1570	40.35	SiH str.
ν_2	a′	1663	74.34	1192	36.31	Bridge HSi str.
ν_3	a′	985	108.22	702	50.30	Bridge H-shift
ν_4	a′	484	17.50	464	19.71	SiGe str.
ν_5	a′	395	7.98	300	4.15	SiH bend
ν_6	a″	123	35.09	90	18.44	Torsion
[4]		SiHGeH ($^1A'$)		SiDGeD ($^1A'$)		
ν_1	a′	2069	131.61	1475	64.78	GeH str.
ν_2	a′	1562	96.73	1114	49.10	Bridge H str.
ν_3	a′	995	107.01	716	58.82	bridge H-shift
ν_4	a′	533	2.25	483	4.28	SiGe str.
ν_5	a′	417	5.64	332	1.68	GeH bend
ν_6	a″	130	34.66	93	17.49	Torsion
[5]		$SiGeH_2$ ($^1A_1$)		$SiGeD_2$ ($^1A_1$)		
ν_1	a_1	2075	63.99	1475	32.15	GeH_2 sym. str.
ν_2	a_1	818	51.39	586	23.12	GeH_2 scissor
ν_3	a_1	429	5.50	427	7.17	GeSi str.
ν_4	b_1	285	2.81	209	1.49	Out of plane
ν_5	b_2	2101	88.52	1499	46.20	GeH_2 asym. str.
ν_6	b_2	211	20.63	156	11.04	GeH_2 rock
[6]		HSiGeH ($^1A'$)		DSiGeD ($^1A'$)		
ν_1	a′	2157	84.83	1553	40.94	SiH str.
ν_2	a′	2083	82.86	1484	44.71	GeH str.
ν_3	a′	614	0.48	453	0.51	SiH, GeH bend
ν_4	a′	449	0.39	446	0.08	SiGe str.
ν_5	a′	196	36.39	140	18.57	GeH, SiH bend
ν_6	a″	167	54.82	119	28.05	Torsion
[1]		SiHGe ($^2A''$)		SiDGe ($^2A''$)		
ν_1	a′	1454	70.07	1042	36.02	SiH str.
ν_2	a′	868	105.11	621	52.60	GeH str.
ν_3	a′	401	0.62	400	0.94	SiGe str.

calculations of vibrational frequencies typically overestimates experimental frequencies depending on the method of *ab initio* calculations (by 2–4% at the B3LYP level). To correct for this deficiency, a useful approach widely utilized is the incorporation of scaling factors, i.e., multiplying the calculated frequency with the scaling factor [45–46]. After the irradiation, the ices were kept at 12 K for one hour and then warmed up at 0.5 K min^{-1} to 293 K. At 22 K, the 2062 cm^{-1} absorption feature split into two peaks, 2072 and 2058 cm^{-1}. These two frequencies were assigned in a previous study to solid state silylgermane [14] and were noted as very strong absorption features. This feature is still observable at 72 K; this implies that these absorptions belong to a stable compound such as the H_3SiGeH_3. The detection of the silylgermane was also confirmed in the deuterated silane–germane ices. An absorption feature at 1462 cm^{-1}, shown in Fig 2(d), was observed corresponding to the ν_2 vibrational modes according to the B3LYP/6-311G(d,p) harmonic frequencies compiled in Table 3, also using a scaling factor of 0.97. This peak is observed at 72 K again implying that this absorption feature belongs to a stable, closed shell compound.

Further investigation of the irradiated silane–germane ice led to the detection of a 550 cm^{-1} band. This feature was observed after 50 min of irradiation and disappears after 60 min. This peak was tentatively assigned to the $H_2GeSiH_3(X^2A')$ ν_7, GeH_2 umbrella,

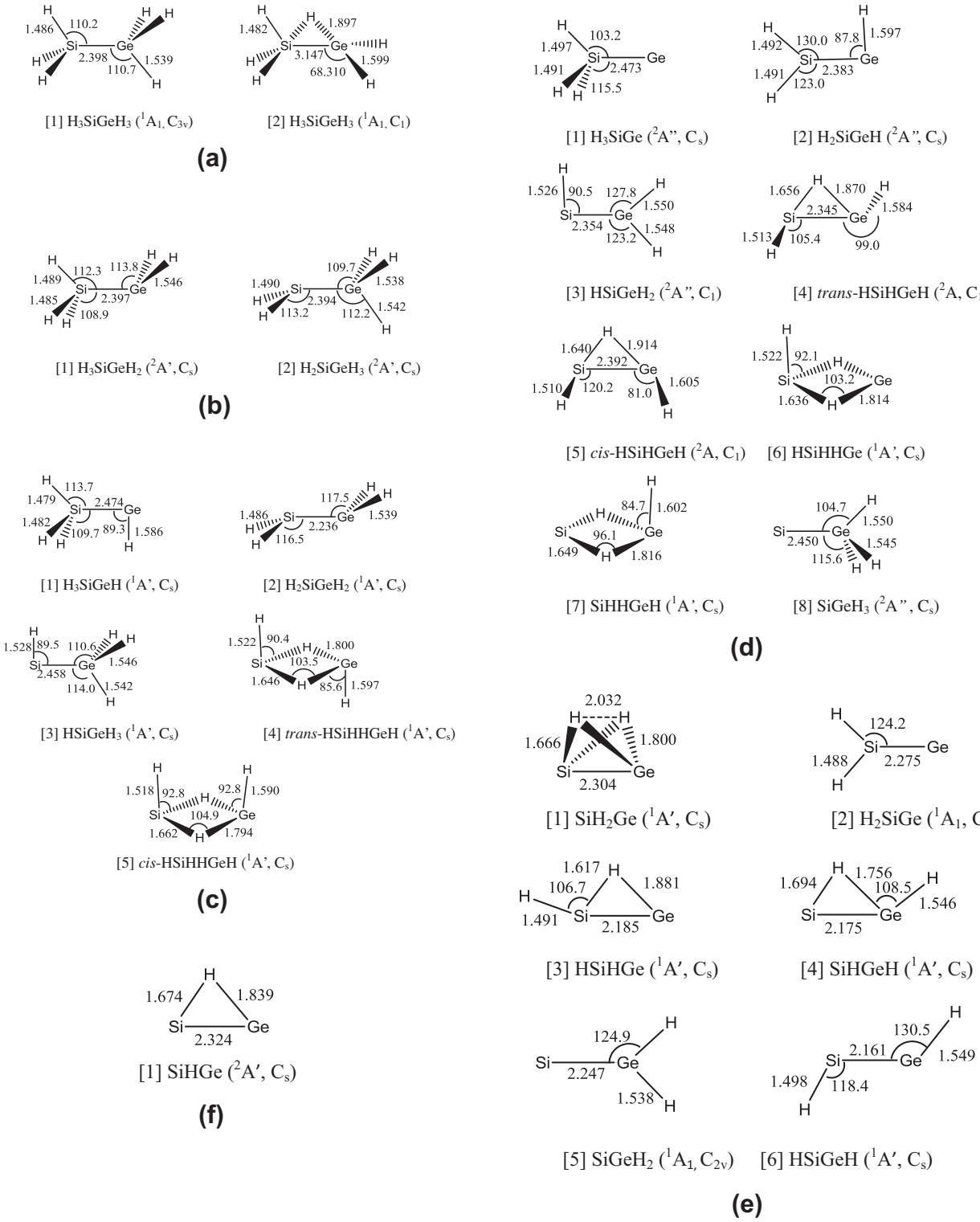

Fig. 1. Optimized structures of (a) $SiGeH_6$, (b) $SiGeH_5$, (c) $SiGeH_4$, (d) $SiGeH_3$, (e) $SiGeH_2$, and (f) SiGeH species at B3LYP/6-311G(d, p) level. The bond lengths and angles are given in units of angstroms and degrees, respectively. Relative energies of $SiGeH_x$ isomers are compiled in Table 2.

SiH_3 rock mode, using the B3LYP calculated harmonic frequencies and scaling factor of 0.97. This absorption feature has a low calculated intensity of 14.07 km mol^{-1} which predicts that this peak would be quite hard to observe. The assignment was confirmed in deuterated silane–germane ice, and a 642 cm^{-1} peak, shown in Fig 2(e) was found, that increased in size after 40 min of irradiation. This was assigned to the D_2GeSiD_3 (X^2A') according to the B3LYP calculated frequency of the ν_5 SiH_3 umbrella mode with scaling factor of 0.97. It should be noted that for this deuterated molecule, this mode has the second highest calculated intensity of 100.93 km mol^{-1}.

Having identified the $H_3SiGeH_3(X^1A_1)$ and, tentatively, the $H_2GeSiH_3(X^2A')$ molecules, further absorptions of the irradiated silane–germane ice were analyzed. An absorption feature at

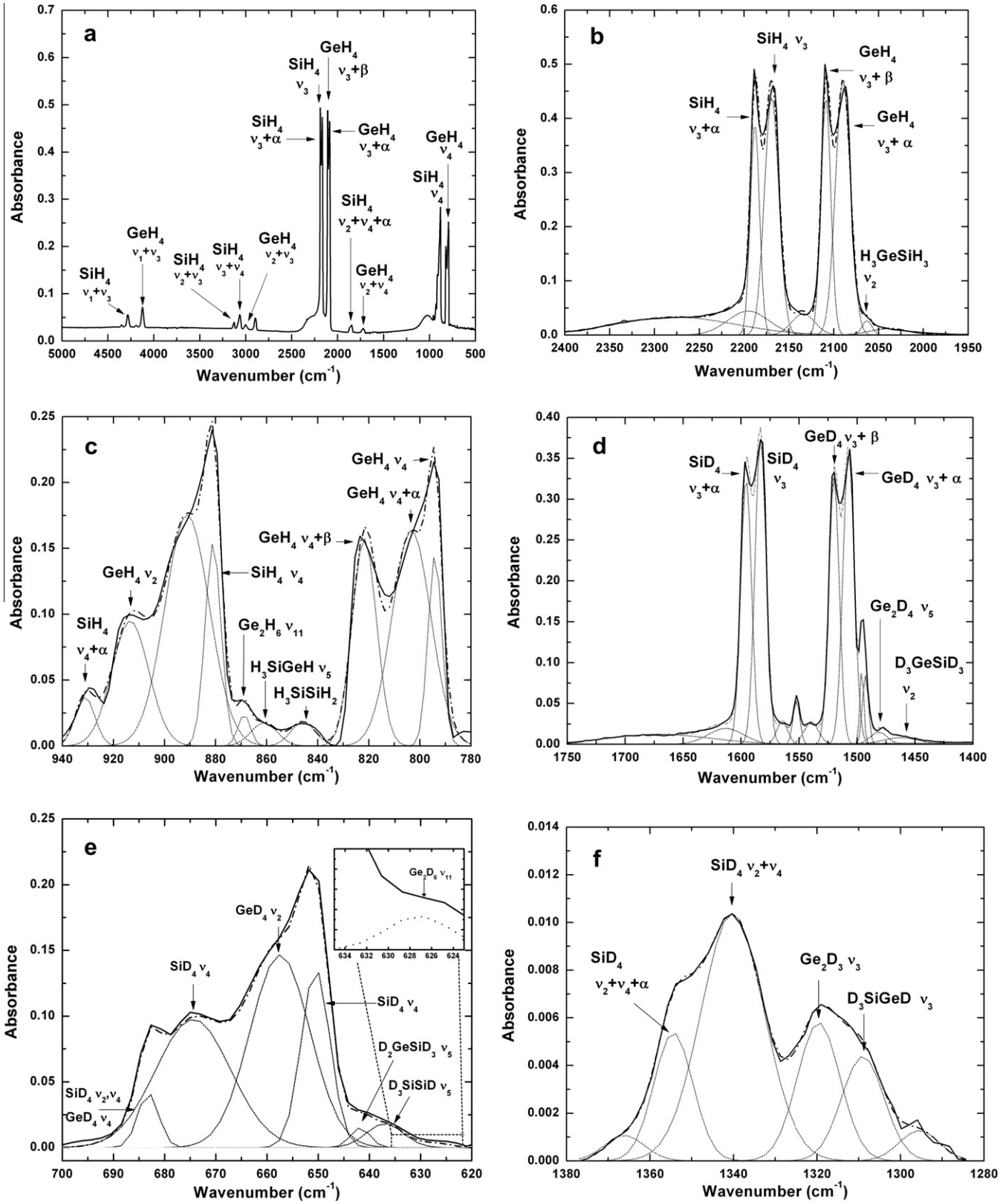

Fig. 2. Infrared spectra of the silane (SiH_4)–germane (GeH_4) frost at 12 K (a). After irradiation, deconvoluted peaks show new absorption features of H_3SiGeH_3 ($^1A_1$) at 2062 cm^{-1} (b), H_3SiGeH ($^1A'$) at 860 cm^{-1} (c), and for the deuterated compounds, D_3SiGeD_3 ($^1A_1$) at 1462 cm^{-1} (d), D_2GeSiD_3 at 642 cm^{-1} (e), D_3SiGeD ($^1A'$) at 1309 cm^{-1} (f).

860 cm^{-1} was found (Fig. 2(c)) suggesting the ν_5 SiH_3 umbrella mode of silylgermylene, $H_3SiGeH(X^1A')$. It should be noted here that the MP2 calculated harmonic frequencies for the silylgermane (H_3SiGeH_3) were compared to the literature experimental frequencies observed previously in the solid state by Lannon et al. al. [14] Scaling factors of 0.93 to 0.94 matched the calculated data with the

Table 4
Observed Ge_2H_x and Si_2H_x species (x = 1–6) and their absorptions in low temperature silane–germane matrices.

Carrier	Frequency (cm^{-1})	Fundamental	Carrier	Frequency (cm^{-1})	Fundamental	Ref.
Si_2H_6	Overlay (820)	ν_6	Si_2D_6	1531	ν_5	[25]
H_3SiSiH_2	844	ν_6	D_3SiSiD_2	621	ν_6	[25]
H_3SiSiH	869	ν_5	D_3SiSiD	635	ν_5	[26]
H_2SiSiH	636	ν_5	D_2SiSiD	Overlay (683)	ν_4	[26]
Ge_2H_6	752	ν_6	Ge_2D_6	530	ν_6	[28]
	869	ν_{11}		626	ν_{11}	[28]
H_2GeGeH_3	766	ν_6	D_2GeGeD_3	609	ν_4/ν_{12}	[28]
			D_2GeGeD_2	1481	ν_5	[27]
H_3GeGeH	780	ν_5	D_3GeGeD	557	ν_5	[28]
H_2GeGeH	1819	ν_3	D_2GeGeD	1319	ν_3	[28]

Table 5
Newly observed species and their absorptions in low temperature silane–germane matrices.

Carrier	Frequency (cm^{-1})	Fundamental	Carrier	Frequency (cm^{-1})	Fundamental
H_3GeSiH_3	2062	ν_2	D_3GeSiD_3	1462	ν_2
H_2GeSiH_3	550[(a)]	ν_7	D_2GeSiD_3	642	ν_5
H_3SiGeH	860	ν_5	D_3SiGeD	1309	ν_3

[(a)] Not shown in Fig. 2.

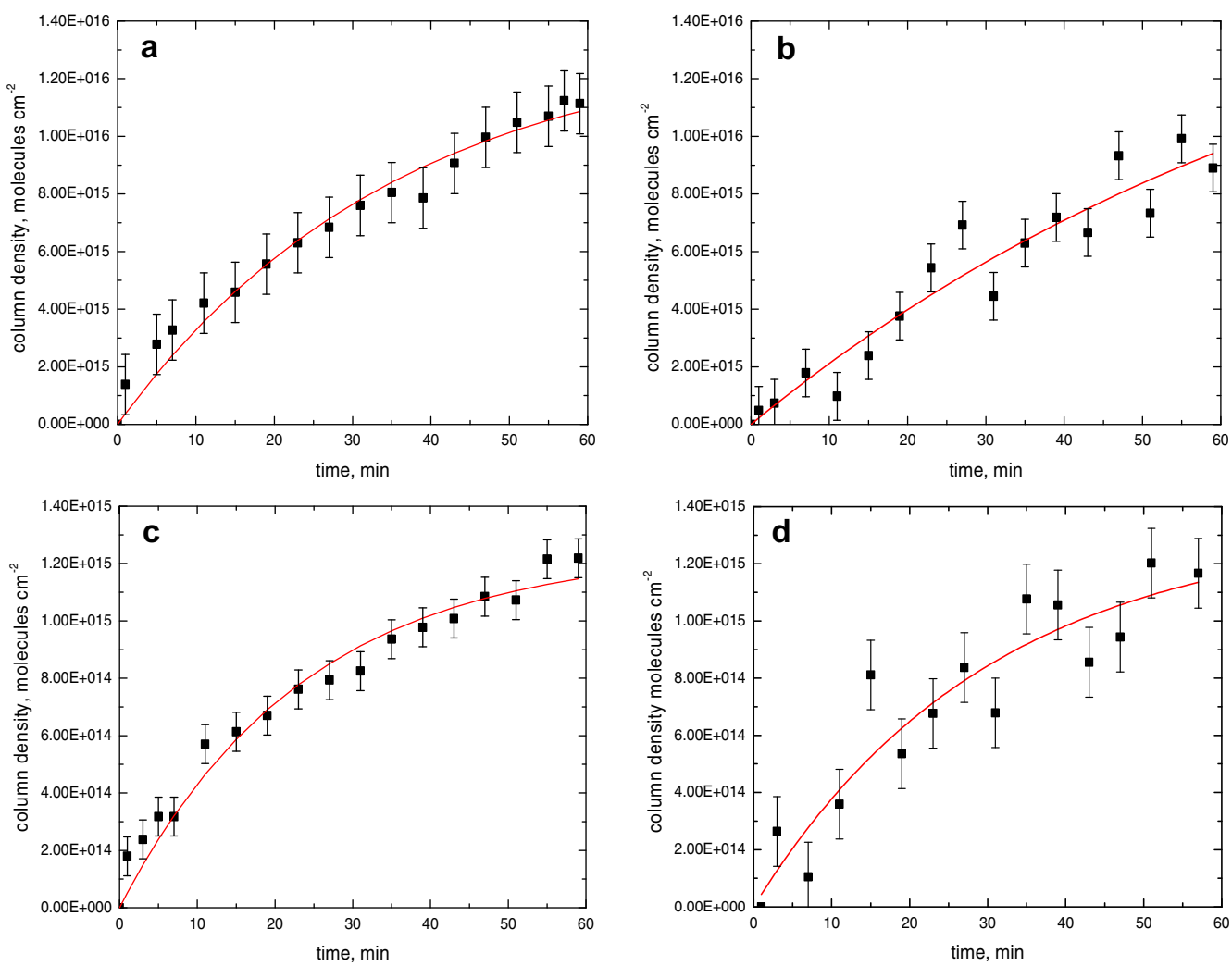

Fig. 3. Temporal evolution of the experimental column densities and the best fits for H_3SiGeH_3 ($^1A_1$) ν_2 (a), D_3SiGeD_3 ($^1A_1$) ν_2 (b), H_3SiGeH ($^1A'$) ν_5 (c), and D_3SiGeD ($^1A'$) ν_3 (d), during irradiation of the silane–germane matrix at 12 K.

experimental observations. These MP2 frequencies were also compared to the vapor state experimental frequencies [14] scaling factors of 0.95 were calculated. An investigation of the deuterated silane–germane ice revealed an absorption feature at 1309 cm^{-1} (Fig. 2(f)). According to the theoretical data, the second most intense frequency for the deuterated silylgermylene is 1316 cm^{-1} ν_3 GeD stretch. It was also observed that the two peaks, 860 and 1309 cm^{-1} both disappear at 52 K upon warming the solid silane–germane ice suggesting a compound less stable than $H_3SiGeH_3(X^1A_1)$. Note that no absorptions for $SiGeH_x$ (x = 1–3) were observed experimentally. In summary, we have detected the silylgermane ($SiGeH_6$) and silylgermylene (H_3SiGeH) molecules along with their deuterated counterparts. We also observed an absorption feature for the H_2GeSiH_3, molecule of which we have made a tentative assignment.

6. Discussion and summary

The theoretical calculations and experiments revealed the formation of silylgermane ($H_3SiGeH_3(X^1A_1)$) and silylgermylene ($H_3SiGeH(X^1A')$) together with their deuterated counterparts. We now attempt to decipher a reasonable reaction mechanism for the two compounds. In a previous work by Carrier et al. of electron irradiated germane ices [27], the authors proposed that the digermane (Ge_2H_6) formation followed a (pseudo) first order reaction mechanism involving first the combination of two neighboring germyl radicals (GeH_3) with correct geometrical orientation within the pure solid germane ice yielding an energized Ge_2H_6 molecule, which was then stabilized by transfer of its internal energy to the surrounding ice. Alternatively, energized Ge_2H_6 molecules can fragment via atomic and/or molecular hydrogen loss pathways forming Ge_2H_5 and Ge_2H_4 isomers, respectively. In the present experiments, we utilized similar reaction scheme (Eq. (2)) to fit the derived temporal profiles.

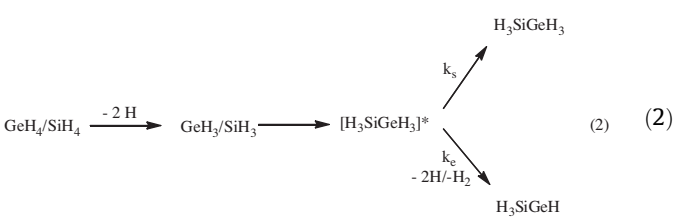

(2)

The temporal evolution of the column densities and inherent fits of the silylgermane ($SiGeH_6$) utilizing the 2062 cm^{-1} band (ν_2 mode) is shown in Fig 3(a). The kinetic fit using (pseudo) first order kinetics (Eq. (3)) with the temporal evolution of the silylgermane, $[A]_t$, yields the best fit with $b = 13 \pm 1 \times 10^{15}$ molecules cm^{-2} and $k = 0.028 \pm 0.004$ min^{-1}.

$$[A]_t = b[1 - \exp(-kt)] \quad (3)$$

Considering the temporal profile and the previously suggested reaction mechanism to form Ge_2H_6, we propose that the silylgermane ($H_3SiGeH_3(X^1A_1)$) molecule is formed via a (pseudo) first order reaction mechanism. This involves the silyl (SiH_3) and germyl (GeH_3) radicals formed via the loss of atomic hydrogen from silane and germane, respectively, within the ice upon irradiation with energetic electrons. If the neighboring radicals have the correct geometrical orientation, they can recombine to form energized silylgermane molecules $[H_3SiGeH_3]^*$, which can then transfer the excess internal energy to the matrix' this effectively stabilized the silylgermane molecule. The deuterated silylgermane ($D_3SiGeD_3(X^1A_1)$) follows the same temporal column density fit, and, therefore we suggest that its formation mechanism is the same as silylgermane and involves the recombination of neighboring D3-silyl and D3-germyl radicals. The kinetic fit using (pseudo) first order kinetics (Eq. (2)) of D6-silylgermane yields the best fit with $b = 12 \pm 6 \times 10^{15}$ molecules cm^{-2} and $k = 0.012 \pm 0.008$ min^{-1}. This slower rate constant in the case of the per-deuterated system might reflect a kinetic isotope effect, i.e., a slower rate of deuterium versus hydrogen elimination in the decomposition of D4-silane and D4-germane. This trend was reported by Kaiser et al. in MeV proton irradiated methane and D4-methane ices at 10 K, where methane was found to decompose more efficiently than D4-methane by a factor of 6 ± 2 [47].

Having proposed the reaction mechanism to form silylgermane ($H_3SiGeH_3(X^1A_1)$), we are turning our attention now to the formation of silylgermylene ($H_3SiGeH(X^1A')$). In a previous work by Carrier et al. [27] the authors recommended that the H_3GeGeH isomer is formed through the unimolecular decomposition of energized digermane by molecular hydrogen elimination. Here, we propose a similar mechanism to form the silylgermylene ($H_3SiGeH(X^1A')$) isomer via energized silylgermane $[H_3SiGeH_3]^*$. The temporal evolution of the 860 cm^{-1} vibrational frequency ν_5 mode and the inherent fit are shown in Fig 3(c), using Eq. (3). The rate constant for this reaction pathway was calculated to be 0.04 ± 0.01 min^{-1} and $b = 1.3 \pm 0.1 \times 10^{15}$ molecules cm^{-2}. These data indicate a (pseudo) first order reaction mechanism involving a unimolecular decomposition of internally excited silylgermane $[H_3SiGeH_3]^*$. The temporal evolution of the 1309 cm^{-1} vibrational frequency ν_3 mode of the perdeuterated counterpart and the inherent fit are shown in Fig 3(d), using Eq. (3). The rate constant for this reaction pathway was calculated to be 0.03 ± 0.01 min^{-1} and $b = 1.3 \pm 0.2 \times 10^{15}$ molecules cm^{-2}. Note that the $H_2GeSiH_3(X^2A')$ radical assigned tentatively via its 550 cm^{-1} absorption might be formed as a transient species at very low concentrations either by radiolysis of silylgermane ($H_3SiGeH_3(X^1A_1)$) or via decomposition of energized silylgermane $[H_3SiGeH_3]^*$. The concentrations are too low to extract quantitative kinetics.

Summarized, we observed the silylgermane ($H_3SiGeH_3(X^1A_1)$) and for the very first time the silylgermylene ($H_3SiGeH(X^1A')$) molecule together with their fully deuterated isotopomers in low temperature silane–germane and D4-silane–D4-germane matrices using infrared spectroscopy. Kinetic fits were presented suggesting that – within the liming of radical recombination reactions – the silylgermylene is formed via a unimolecular decomposition of energized silylgermane molecules.

Acknowledgments

This work was supported by the US National Science Foundation (CHE-0948258). Computer resources at the National Center for High-performance Computer of Taiwan were utilized in the calculations.

References

[1] B.S. Meyerson, vol. 270 (iii), Scientific American, 1994, pp. 42.
[2] A. Potie, T. Baron, F. Dhalluin, G. Rosaz, B. Salem, L. Latu-Romain, M. Kogelschatz, P. Gentile, F. Oehler, L. Montes, Nanoscale Res. Lett. 6 (2010) 187.
[3] G. Chen, G. Springholz, W. Jantsch, F. Schaeffler, App. Phys. Lett. 99 (2011) 43103.
[4] K. Ismail, B.S. Meyerson, P.J. Wang, Appl. Phys. Lett. 58 (1991) 2117.
[5] T. Hackbarth, G. Hoeck, H.J. Herzog, M. Zeuner, J. Crys, Growth 201 (1999) 734.
[6] R. People, J.C. Bean, C.G. Bethea, S.K. Sputz, L.J. Peticolas, Appl. Phys. Lett. 61 (1991) 1122.
[7] P. Sun, S. Chang, Y. Chen, H. Lin, Solid-State Electron. 54 (2010) 1216.
[8] Y.S. Tang, W.X. Ni, C.M. Torres, G.V. Hansson, Electron. Lett. 31 (1995) 1385.
[9] K. Washiro, IEEE Trans. Electron. Devices 50 (2003) 656.
[10] A. Stosic, V. Markovic, Z.J. Marinkovic, Autom. Control 16 (2006) 25.
[11] J.D. Cressler, R. Krithivasan, A.K. Sutton, J.E. Seiler, J.F. Krieg, S.D. Clark, A.J. Joseph, IEEE Trans. Nucl. Sci. 50 (2003) 2086.
[12] G. Patton, S. Iyer, S. Delage, S. Tiwari, J. Stork, Proc. – Electrochem. Soc. 88 (1988) 114.
[13] W.D. de Boer, D.J. Meyer, Appl. Phys. Lett. 58 (1991) 1286.
[14] E.J. Spanier, A.G. MacDiarmid, Inorg. Chem. 2 (1963) 215.
[15] F.W. Lampe, Spectrochim. Acta Part A 43A (1987) 257.
[16] J.A. Lannon, G.S. Weiss, E.R. Nixon, Spectrochim. Acta 26A (1970) 221.

[17] S. Mohan, A.R. Prabakaran, F. Payami, J. Raman, Spectrosc. 20 (1989) 119.
[18] S. Mohan, M. Baskaran, Spectrochim. Acta 46A (1990) 757.
[19] H. Obenhammer, T. Lobreyer, W. Sundermeyer, J. Mol. Struct. 323 (1994) 125.
[20] P. Gaspar, J.J. Frost, J. Am Chem, Soc. 95 (1973) 6567.
[21] F.E. Saalfeld, H.J. Svec, J. Phys. Chem. 70 (1966) 1753.
[22] J.O. Jensen, Spectrochimic. Acta Part A 59 (2003) 3093.
[23] J. Urban, P. Schreiner, G. Vacek, P. Von Rague Schleyer, J. Huang, J. Leszczynski, Chem. Phys. Lett. 264 (1997) 441.
[24] R.S. Grev, H.F. Schaefer III, K.M. Bainess, J. Am. Chem. Soc. 112 (1990) 9458.
[25] D. Sillars, C. Bennett, Y. Osamura, R. Kaiser, Chem. Phys. Lett. 305 (2004) 141.
[26] D. Sillars, C. Bennett, Y. Osamura, R. Kaiser, Chem. Phys. Lett. 392 (2004) 541.
[27] W. Carrier, W. Zheng, Y. Osamura, R. Kaiser, Chem. Phys. 330 (2006) 275.
[28] W. Carrier, W. Zheng, Y. Osamura, R. Kaiser, Chem. Phys. 325 (2006) 499.
[29] C. Bennett, A.M. Mebel, R.I. Kaiser, Phys. Chem. Chem. Phys. 6 (2004) 735.
[30] A.M. Coats, D.C. McKean, D. Steele, J. Mol. Struct. 320 (1993) 269.
[31] A.D. Becke, J. Chem. Phys. 98 (1993) 5648.
[32] A.D. Becke, J. Chem. Phys 96 (1992) 2155.
[33] A.D. Becke, J. Chem. Phys. 97 (1992) 9173.
[34] C. Lee, W. Yang, R.G. Parr, Phys. Rev. B 37 (1988) 785.
[35] G.D. Purvis, R.J. Bartlett, J. Chem. Phys. 76 (1982) 1910.
[36] C. Hampel, K.A. Peterson, H.J. Werner, Chem. Phys. Lett. 190 (1992).
[37] P.J. Knowles, C. Hampel, H.J. Werner, J. Chem. Phys. 99 (1994) 5219.
[38] M.J.O. Deegan, P.J. Knowles, Chem. Phys. Lett. 277 (1994) 321.
[39] M.J. Frisch et al., GAUSSIAN 03, Revision C.02, Gaussain, Inc., Wallingford CT, 2004.
[40] R. Walsh, Acc. Chem. Res. 14 (1981) 246.
[41] K. Brady Clark, D. Griller, Organometallics 10 (1991) 746.
[42] H. Lischka, H.J. Kohler, J. Am. Chem. Soc. 10 (1983) 6646.
[43] R.I. Kaiser, Y. Osamura, Astron. Astrophys. 432 (2005) 559.
[44] G. Gopakumar, V.T. Ngan, P. Leviens, M.T. Nguyen, J. Phys. Chem. 112 (2008) 12187.
[45] A.P. Scott, L. Radom, J. Phys. Chem. 100 (1996) 16502.
[46] G. Rauhut, P. Pulay, J. Phys. Chem. 99 (1995) 3039.
[47] R.I. Kaiser, G. Eich, A. Gabrysch, K. Roessler, Astrophysics 484 (1997) 487.